Martínez, M.; Altantzis, C.; Wright, YM.; Marti-Aldaravi, P.; Boulouchos, K. (2022). Computational study of the Premixed Charge Compression Ignition combustion in a Rapid Compression Expansion Machine: Impact of multiple injection strategy on mixing, ignition and combustion processes. Fuel. 318:1-16. https://doi.org/10.1016/j.fuel.2022.123388

Martinez et al. "Computational study of the PCCI combustion in a RCEM: Impact of multiple injection strategy on mixing , ignition and combustion processes," Fuel, vol. 318, no. January, p. 123388, 2022. DOI: 10.1016/j.fuel.2022.123388

Computational study of the Premixed Charge Compression Ignition combustion in a Rapid Compression Expansion Machine: Impact of multiple injection strategy on mixing, ignition and combustion processes.

María Martínez[a], Christos Altantzis[b], Yuri M. Wright[b,c], Pedro Martí-Aldaraví[a], Konstantinos Boulouchos[b]

[a] *CMT-Motores Térmicos, Universitat Politècnica de València*
[b] *Aerothermochemistry and Combustion Systems Laboratory, Swiss Federal Institute of Technology, Zurich, Switzerland*
[c] *Combustion and Flow Solutions GmbH, Zurich, Switzerland*

Abstract

Combustion processes operating under the low-temperature (LTC) are a promising alternative for internal combustion engines, achieving high efficiency and low emissions within the legislative framework. Under this field of study, the concept of Premixed Charge Compression Ignition (PCCI) was introduced to control the combustion phase by varying the injection strategy. The present research, based on the aforementioned combustion strategy, employs Computational Fluid Dynamics (CFD) to study the mixing, ignition and initial combustion processes in a Rapid Compression and Expansion Machine (RCEM). The operating conditions of the PCCI strategy are achieved through the split injection technique, which separate the injection into several shots. In this case, the injection strategy consists of a long base injection and two very short, consecutive post injections delivered when the piston is close to the top dead center. Three different operating conditions have been considered which differ mainly in the duration and the starting time of the first injection. Large Eddy Simulations (LES) are selected to account for the effects of turbulence. Results are validated against experimental data, showing good agreement between both approaches. The effect of the first injection on the second one in multiple injection strategy is appreciated as the penetration of the subsequent fuel sprays is faster. Differences in the

local mixture field and ignition dynamics are observed as a function of varying operating conditions. The ignition process is highly influenced by the operating strategies affecting the distribution of the mixture and thus the location of the low temperature oxidation. In the current computational study, in addition to the evaporating fuel scalar, the corresponding source term due to evaporation has also been provided to three passive transported scalars, namely three mixture fractions, one for each injection event. This allows for discerning the fuel stemming from each one of the pulses in the overall distribution, thus offering new insights into the effect of the injection strategy.

Keywords: Premixed Charge Compression Ignition, Rapid Compression and Expansion Machine, CFD, Large Eddy Simulation, mixing and ignition dynamics

1. Introduction

In recent decades, public concern on the increase of air contamination and the reduction of fuel resources has risen. This has provoked governments to further tighten regulations of the homologation tests [1, 2]. The regulations on the level of pollution and CO_2 emitted by combustion engines to the atmosphere combined with ongoing quest to enhance engine efficiency, prompted the scientific community to explore alternative methods to traditional combustion systems that are capable of meeting current and future requirements. In this context, one of the most promising alternatives is the application of low temperature combustion (LTC) concepts for direct-injection diesel engines [3]. LTC modes are characterized by highly diluted mixtures in effort to decrease the overall temperature of the combustion process. Consequently, complete combustion is achieved by controlling the physical and chemical processes of the air-fuel mixture and ignition timing. Therefore, LTC has been described by researchers as an interesting approach to increase thermal efficiency and minimize NO_x formation and soot emissions [4, 5]. Under this field of study, the concept known as Homogeneous Charge Compression Ignition (HCCI) has potential to improve efficiency. The HCCI concept has the advantage of being applied in either compression ignition (CI) or spark ignition (SI) engines [6, 7]. Usually, a homogeneous lean air–fuel mixture is created due to the premixed process. It ignites automatically in several locations and is then burned volumetrically without visible flame propaga-

tion [8]. Once ignited, combustion takes place very rapidly and is completely governed by chemical kinetics rather than the mixing rate in CI engines or the turbulent flame propagation speed in SI engines. Although HCCI is beneficial in terms of efficiency and emissions, it has some drawbacks such as a higher rate of pressure increase, lack of control of the combustion phase, unburned hydrocarbons (UHC) and a limited operating load range [9]. In order to extend the operating load range in HCCI, numerous alternatives are provided such as the use of exhaust gas recirculation (EGR) [10], intake air preheating [11], variable compression ratio [12], supercharging [13] and water injection [14, 15]. Since the ignition timing and the combustion process are mainly determined by the composition of the fuel, it is very challenging to achieve accurate control of the ignition timing. Consequently, the concept of Premixed Charge Compression Ignition (PCCI) was introduced to overcome the major weaknesses of the HCCI in terms of inadequate combustion phases and limits of operability [16]. This approach, unlike the HCCI, has some control over combustion by varying the injection strategy.

The PCCI combustion concept is mainly focused on separating the start of injection from the start of combustion (ignition delay), so that a uniform mixture environment can be reached before ignition occurs. This strategy avoids local rich areas and, thereby, resulting in low soot emissions [17]. PCCI operating mechanism is based on combining very early or late injection timing, high injection pressure, low compression ratio and high levels of EGR. All these strategies allow the combustion process to occur at low temperature below the NO_x formation range. As it is already known, PCCI strategy has a hybrid operation between conventional and HCCI combustion modes so that the limiting processes are modified by the kinetic characteristics or the injection strategy [18]. The present research is focused on the study of the mixing and ignition behavior when a PCCI strategy is used and multiple injections are applied to control the combustion phase.

Over the last years, many studies have focused on analysing LTC models both experimentally and computationally. Desantes et al. [19, 20] performed autoignition propagation analysis under HCCI conditions using a rapid compression expansion machine (RCEM). They determined the ignition delay of pure fuels as well as of different mixtures and evaluated the velocity and the characteristic duration of combustion process. Kokjohn et al. [21] investigated the potential of controlling premixed charge compression ignition (PCCI and HCCI) combustion strategies by varying fuel reactivity through the dual-fuel technique. Their findings suggested that the overall fuel reac-

tivity is able to control the combustion phase, but it is necessary to stratify the fuel reactivity to control the rate of heat release as the load increases. These studies were focused not only on the analysis of reaction kinetics but also on the injection strategy. Advanced direct injection systems are flexible and enable the injection to be divided into several pulses during an engine cycle. Multiple injection strategies are one of the numerous technologies implemented in modern diesel engines to improve its pollutant emissions and high combustion noise by reducing the rate of pressure rise [22–24]. Furthermore, this method of injection improves the air-fuel mixture in the cylinder and prevents effects such as fuel wetting on the piston walls [25]. Payri et al. [26] carried out studies based on multiple injections in a constant pressure and flow vessel supported with one dimensional CFD analysis. They demonstrated that the first pulse accelerates the stationary gas in the combustion chamber, thereby the second event loses less axial momentum and penetrates faster than the reference single injection case. Mathivanan et al. [27] evaluated the effect of changing the fuel injection quantity and timing on the performance. Their research showed about 15% improved thermal efficiency and 24% lower smoke emission when employing multiple injections in comparison with the single injection case. Additionally, they found that retarding the timing and reducing the duration of the last injection pulse decrease the NO_x emission levels. Lu et al. [28] compared single with multiple fuel injection in a PCCI engine. The studies were not only carried out experimentally but also served for simulation validation. At low loads, there were no differences in mixture formation, emissions, and thermal efficiency between both injection strategies. On the contrary, at high loads and compared to single injection, a lean and homogeneous mixture formation is experienced using multiple fuel injection. In a recent study, Doll et al. [3] experimentally measured the mixing dynamics for several split injection strategies in a RCEM and assessed their relation to the ignition characteristics of each case.

The studies presented above, carried out both experimentally and computationally, demonstrate that many efforts have been conducted to understand the behavior of LTC concepts, as well as the influence of multiple injections on the mixing and combustion process. However, the addressed results were mostly achieved at constant ambient densities and therefore lack the transient behavior of a real engine cycle. In addition, the above mentioned investigations are focused on the interaction between subsequent injections without taking into account the operational characteristics required for PCCI strategies, such as mixture preparation. To the best knowledge of the authors

none of the computational studies has modeled the geometry in detail. It is well recognized that a computational simulation is able to reduce research and development times as well as complement experimental findings by providing knowledge not available in the experiments. For all these reasons, the objective and main originality of the present research is the detailed understanding of the flow phenomena occurring during a split injection PCCI taking into account the transient behavior of a full engine cycle, focusing on the analysis of the preparation of the mixture and the combustion behavior. This allows explaining the experimental observations and confirming the previously drawn hypothesis. The setup follows the detailed experimental campaign employed in previous researches [3]. The survey will be carried out computationally on a RCEM which will be operated with a split injection PCCI strategy. For this purpose, a prototype of detailed geometry close to reality has been used so that all the effects and behavior of the fluid can be accurately reproduced. High fidelity simulations, where existing turbulence is addressed from Large Eddy Simulation (LES) approach, will be performed in order to analyze the characteristics of the mixing formation during the injection process. The research includes the evaluation of the mesh quality to ensure precision in the results and focuses on spray behavior, local mixing phenomena as well as in-depth thermodynamic analysis of global heat release rates, the ignition process and fuel consumption. The present work not only seeks precision in the results and validate them with experimental data but also to demonstrate the capabilities of the models and sub-models involved in the study and the limitations they have.

2. Problem description

2.1. Geometry - Rapid Compression and Expansion Machine

The RCEM is an experimental free floating piston device capable of reproducing certain engine operating phases such as compression or initial expansion with the advantage of greater control of initial and boundary conditions [29]. One of the main strengths of this facility is the wide range of engine operating conditions that can be tested and the easy optical access. Only by varying the oil or air volume can critical combustion parameters such as compression ratio or piston speed be controlled. The particular RCEM of study, presented in Figure 1, has a modular design which allows to customize the machine according to the desired test. It has two clearly differentiated parts:

the experimental area composed by the combustion chamber where the optical accesses for the experiments are placed and the driving zone made up of four different pistons and corresponding to the mechanical part. The pushing piston, colored in blue in Figure 1, is pneumatically driven and hydraulically coupled to the experimental/driver piston which is directly connected to the combustion chamber. The stroke piston, colored in red in Figure 1, is hydraulically driven and can be adjusted to select the compression stroke. The last piston, marked in light blue in Figure 1, contains the compressed air that drives the machine by pushing the piston to the cylinder head.

The working principle of the RCEM is as follows: first, the driving gas composed of compressed air pressurizes the oil. The driver piston is kept immobile thanks to the perfect coupling with the stroke piston. Pressure is then established downstream of the driver piston by means of a bypass valve and the piston progresses at low speed in a slow compression process. The oil volume should be kept constant so when the driver piston advances, the pushing piston must also progress in the opposite direction. The driver piston is suddenly accelerated and the rapid compression stroke starts when it leaves the stroke piston. The driven air as well as the pushing oil reduces its pressure due to the suffered expansion process. The piston stops its motion when the pressure inside the combustion chamber is sufficiently high to balance the pushing force and inertia, defining the TDC. TDC is highly dependent on the operating conditions, and there is also a certain maximum driving pressure for each operating condition to avoid piston collision with the cylinder head. Once the piston reaches TDC, the pressure inside the combustion chamber is greater than the pushing oil pressure and the expansion stroke begins. A broader explanation of the RCEM operating principles can be found at previous works [30–33].

The RCEM available at ETH-Zürich is originally designed by Testem and subsequently modified (i.e. equipped with a liner heating and modified piston and cylinder head(s)). Among its technical characteristics, highlight the steel-made piston with 84 mm of bore and a quartz-made bowl with cylindrical shape, 50 mm of bore and 2.2 mm of depth, which allows the axial optical access. The flat shape of the bowl enables to capture images without distorting them. Furthermore, it also has an optical access of 40 mm in diameter at the side. The stroke can be varied from 120 to 249 mm being selected for the current study 245 mm. The compression ratio can be operated between 5 and 30 and the maximum achievable pressure in the cylinder is 200 bar. Further operational characteristics can be found in recent

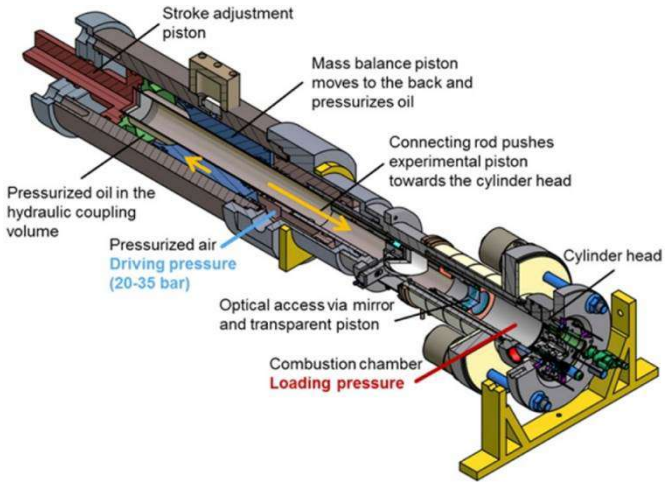

Figure 1: Schematic diagram of the RCEM: the compressed air drives the mass-balance piston, accelerating the working piston towards the cylinder head. Adapted from [3].

publications [30, 34–36]. The employed injector is of solenoid type used and characterized in previous studies [37] and mounted on the cylinder periphery (5 mm below the flat cylinder head, 42.5 mm from the cylinder axis and inclined 5º towards the piston).

2.2. Operating conditions - Multiple injection strategy

Multiple injection procedures, including pilot and post injections, are referred to as useful means not only for traditional diesel combustion but also for diesel PCCI combustion to regulate the exhaust emissions. This research focuses on the analysis of the PCCI strategy together with the use of multiple injections. The implementation of post injections has been chosen for this study. Within post injections there are several strategies commonly employed: single and double post injections. Both contribute to a significant reduction in HC and CO as they encourage the complete combustion of the unburned species. Some studies such as the one carried out by Park [38] demonstrated a greater efficiency in reducing these unburned species with the use of double injection posts due to the reduction of the distance of penetration of the aerosol by the division of the injection post. That said, the present work focuses on the use of a long main injection to provide an adequate air-fuel mixture in the combustion chamber followed by a post injection splitted into two small pulses tightly spaced to TDC.

This article presents three different operating conditions which aim to study diverse states of mixing at ignition while respecting the operating limits of the machine (RCEM). These operating conditions have been designed in [3] so that combustion takes place at low temperatures before the last injection was partially premixed. Although computationally it is possible to visualize the behavior of the flow throughout the entire domain, this is not the case in experiments where optical access is limited. For this reason, the operating conditions have been set so that the mixing and ignition process are visible through the optical accesses of the RCEM. The mentioned conditions, which follow the experimental nomenclature [3], are summarized in Figure 2. The upper part of this image additionally represents the average in-cylinder pressure as well as the position of the piston at the reference condition.

Diesel fuel consists of a complex mixture of hundreds of hydrocarbons that differ according to crude oil sources, refining processes, regulations and other factors. Furthermore, diesel fuel contains many fluorescing components, precluding the application of PLIF diagnostics for experimental studies. Therefore, researchers developed alternative fuels to emulate the physical and chemical properties of diesel fuels in order to simplify the study [39]. For this research and with the purpose of shedding light on the interaction between mixing and auto-ignition, n-heptane is used as surrogate mono-component fuel known for its diesel-like cetane characteristics. In addition, employing n-heptane further avoids any influence from of multi-component evaporation. The material properties of the liquid and gaseous species were obtained from the software's own database [40]. The injection pressure used for all operating conditions is established to 600 bar and the back pressure is set to the same value of 2 bar for OPs 1, 2 and 4. Since the first injection event occurs very early, the back pressure in the chamber is correspondingly very low, leading to large penetration and substantial spray-wall impingement as discussed. The low injection pressure was chosen to minimize this effect. Lowering the pressures further was however found to lead to ballistic behavior of the needle, especially for the short pulses close to TDC. That operating condition represents realistic operating conditions for very early injections in the engine. Regarding the piston wall temperature, it has a experimental prescribed value of 378 K for all conditions. The cylinder liner and head as well as the piston are heated using multiple heating elements and a closed loop control with multiple thermocouples at different locations is employed as discussed in [3]. Concerning the injected mass, same energizing time and therefore same injected mass has been defined in the main

injection for OPs 1 and 4. However, OP2 has twice the energizing time of the previous ones, thus increasing the total mass injected. The total mass injected has been listed in Table 1 for the three operating conditions and the different injections in each of them. In the OPs 1 and 2 the main injection starts early in the compression stroke thus increasing the ignition delay and allowing the air-fuel mixture in the chamber. In order to see the effect of delaying the main injection, OP4 has been defined as 10 ms out of phase with the rest of the conditions. The start of injection and the duration of the splitted post injections, which means second and third injection, are the same for all engine conditions. All of the above modifications to the operating conditions have an effect on the global compression ratio being 10.5 for OPs 1 and 4 and 9.9 for OP2. This phenomenon is owing to the existence of a free-floating piston in the RCEM.

Op. Condition	**Injected Fuel Mass [kg]** (1^{st} / 2^{nd} / 3^{rd})	**Total Inj. Mass [kg]**
OP1	8.8125e-06 / 7.93125e-07 / 7.93125e-07	1.039875e-05
OP2	1.7625e-05 / 7.93125e-07 / 7.93125e-07	1.921125e-05
OP4	8.8125e-06 / 7.93125e-07 / 7.93125e-07	1.039875e-05

Table 1: Respective injected fuel mass for each injection strategy (first main injection / second injection / third injection).

3. Computational Methodology

3.1. Model equations

The computational analysis presented in this research was carried out using the CFD software CONVERGE v2.4, a commercial code developed mainly for Internal Combustion Engine (ICE) simulations and based on finite volume methods. The current study is simulated in an Eulerian-Lagrangian framework governed by the classical equations of mass, momentum, species, energy and turbulence. Furthermore, this analysis also describes the physics of fuel spray through a Discret Droplet Model (DDM) approach. This implies that the software provides a Lagrangian approach to capture the liquid droplet dynamics, spray breakup, heat transfer, evaporation, collision, etc. However, both the ambient gas and the vapor phase are solved using an Eulerian framework. The different sub-models mentioned above used for this study are listed in Table 2 and explained in more detail below.

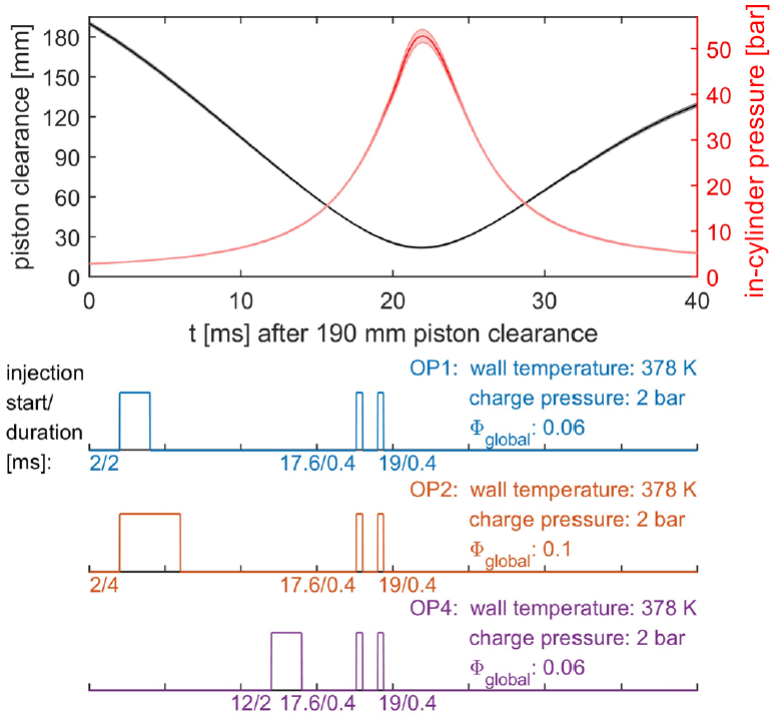

Figure 2: (Top) Ensemble averaged time traces of piston clearance and pressure at reactive OP1. Shaded areas denote cycle-to-cycle experimental variations. (Bottom) Injection strategies for investigated OPs. Respective timings (start of injection/duration) as well as the pressures and temperatures of each operating condition are also indicated. Adapted from [3].

A pressure-velocity coupling iteration method known as Pressure Implicit with Splitting of Operators (PISO) was selected to solve sequentially the transport equations. Rhie-Chow algorithm [41] is used to prevent the decoupling pressure-velocity originated by the location of the transportation quantities at the center of the cell. The discretization scheme used for computing the convection flux in density, energy, species and passives transport equations is second-order central difference scheme whereas the first-order upwind discretization is used for the turbulence. The use of a successive over-relaxation (SOR) algorithm allows to obtain better numerical stability. The time-step is controlled by the Courant-Friedrichs-Lewy (CFL) and result between 10^{-3} and 10^{-10} s. Values for velocity-based Courant-Friedrichs-Lewy (CFL) are below 1 and for viscosity-based CFD below 2.

Physical Model	**Specific Model**
Turbulence model	Viscous One Equation
Heat transfer model	O'Rourke and Amsden
Atomization model	Modified KH-RT
Spray-wall interaction	Wall film
Drag model	Dynamic drop drag
Evaporation model	Frössling
Fuel impact model	NTC collision
Combustion model	SAGE

Table 2: Physical sub-models defined for the present study.

3.1.1. Turbulence model

Over the years the use of LES for turbulence modelling has become widespread. Researchers such as Kakaee et al. [42] demonstrated that although Reynolds Averaged Navier-Stokes (RANS) models were good enough for capturing overall qualitative flow trends, LES models are more accurate in estimating velocity magnitudes, flow structures, turbulence magnitudes and its distribution. Therefore, and with the aim of achieving greater precision in the results, this work has focused on the use of LES methods in which the fields are decomposed into a resolved field and a sub-grid field. First of all, the spatial filtering operation is applied. Then, the unclosed non-linear term of the Navier-Stokes equation is modeled. If LES decomposition is applied to the momentum equation, the filtered transport equation looks like:

$$\frac{\partial \bar{\rho}\widetilde{u}_i}{\partial t} + \frac{\partial \bar{\rho}\widetilde{u}_i\widetilde{u}_j}{\partial x_j} = -\frac{\partial \bar{P}}{\partial x_i} + \frac{\partial \bar{\sigma}_{ij}}{\partial x_j} - \frac{\partial \tau_{ij}}{\partial x_i} \tag{1}$$

Being the terms with '$-$' and '$\backsim$' the filtered quantities obtained through the Reynolds filtering and Favre-filtering, respectively. The variables of density (ρ) and pressure (p) are Reynolds filtered, whereas velocity (u_i) and other thermodynamics variables are Favre-filtered to take into account the compressibility of the fluid [43]. An additional sub-grid model is necessary to close the τ_{ij} defined as the stress flux tensor at the sub-grid. σ_{ij} is the stress tensor expressed by,

$$\bar{\sigma}_{ij} \cong \widetilde{\sigma}_{ij} = \mu(\frac{\partial \widetilde{u}_i}{\partial x_j} + \frac{\partial \widetilde{u}_j}{\partial x_i}) - \frac{2}{3}\mu\frac{\partial \widetilde{u}_k}{\partial x_i}\delta_{ij} \tag{2}$$

For this particular study the One-Equation Viscosity Model [44, 45] sub-grid model has been chosen for the closure. This LES model is characterized for providing an additional transport equation for the sub-grid kinetic energy. Furthermore, it should also be noted that sub-grid kinetic energy is used for modeling the turbulent viscosity. The sub-grid kinetic energy equation is given by

$$\frac{\partial k}{\partial t} + \bar{u}_i \frac{\partial k}{\partial x_i} = -\tau_{ij} \frac{\partial \bar{u}_i}{\partial x_j} - \epsilon + \frac{\partial}{\partial x_i}(\frac{\nu_t}{\sigma_k} \frac{\partial k}{\partial x_i}) \tag{3}$$

Here the sub-grid kinetic energy is defined as

$$k = \frac{1}{2}(\overline{u_i u_i} - \bar{u}_i \bar{u}_i) \tag{4}$$

The sub-grid stress tensor is modeled by

$$\tau_{ij} = -2\nu_t \bar{S}_{ij} + \frac{2}{3} k \delta_{ij} \tag{5}$$

being the turbulent viscosity, ν_t, for the one-equation model denoted as

$$\nu_t = C_k k^{1/2} \Delta \tag{6}$$

where C_k is defined as 0.05 [45] for the current analysis but can be adjusted by the user if necessary. In this framework, Δ is considered the grid filter being the computational cell which determines the size and shape. In the following study and due to the shape of the mesh, the type of filter will be a box. The sub-grid dissipation is defined as

$$\varepsilon = \frac{C_\varepsilon k^{3/2}}{\Delta} \tag{7}$$

This sub-grid dissipation can also be tuned by adjusting the constant C_ε in the previous equation. For the present research, the value equals to 1 [44].

3.1.2. Atomization model

For the present study, the conventional and most commonly used method for simulating disperse liquid sprays known as Discrete Droplet Model Sprays (DDM) is selected. This DDM approach is based on the injection sub-model called blob method which injects an initial drop of the size equivalent to the effective nozzle diameter and that it follows a velocity depending on a mass flow rate profile. For the atomization process modified Kelvin-Helmholtz

(KH) and Rayleigh-Taylor (RT) breakup mechanisms [46] are adopted. This modified version is characterized for not using an *ad hoc* breakup length definition. Child drops are consequence of the primary atomization governed by aerodynamic instabilities (KH model). After that, the secondary breakup is computed by both KH and RT mechanisms. The code verifies whether the RT mechanism is capable of breaking the droplet, if not the KH model is in charge of the breakup.

Kelvin Helmholtz instabilities are due to the slip velocity of the droplet which split the parent droplet into small ones. The radius rate change of the parent droplet is associated to the following equation:

$$\frac{dR}{dt} = \frac{R - R_c}{\tau_{KH}} \tag{8}$$

where R_c corresponds to the diameter of the child droplets and the breakup time is defined as:

$$\tau_{KH} = \frac{3.726 B_1 R_c}{\Lambda_{KH} \Omega_{KH}} \tag{9}$$

Λ_{KH} and Ω_{KH} are the wavelength and growth-rate of the instabilities, respectively. B_1 is defined as a calibration coefficient and was set at 7 for the present work.

Kelvin Helmholtz breakup is considered to be inside the stripping regime whereas the Rayleigh-Taylor breakup is included in the catastrophic regime. The instabilities caused by the RT breakup model tend to accelerate the droplets leading them to pulverize the liquid core completely. The above-mentioned instabilities are described by characteristic time-scale and length-scale as:

$$\tau_{RT} = \frac{C_\tau}{\Omega_{RT}} \tag{10}$$

$$D_{RT} = C_{RT} \Lambda_{RT} \tag{11}$$

Both C_{RT} and C_τ parameters are constants which can be modified according to atomization requirements. C_{RT} could increase or decrease to change the size of the predicted RT breakup radius in the same way as RT time constant C_τ can be increased to delay RT breakup, or decreased to promote faster RT breakup. For the present analysis, these time and size constants have been defined as 1 and 0.1 respectively.

The dynamic drag model is selected to account the effects of drop distortion due to its velocity relative to the continuous phase. The collision effect has also been taken into account in this study choosing the faster collision method, No Time Counter (NTC) of Schmidt and Rutland [47]. After the collision occurs and based on the conditions at the impact time, the outcome of the collision can result in bouncing, stretching separation, reflexive separation, or coalescence [48].

3.1.3. Combustion model

Among all the combustion models available in the literature, the SAGE model [49] has been chosen for this research. This combustion model stands out for solving detailed chemistry based on Arrhenius type correlation. The CFD code is responsible for the transport equations while SAGE model calculates the reaction rates of each primary reaction. For a specific computational cell and at each time-step, the governing equations for mass and energy conservation are solved and the species appropriately updated.

The present work gathers the analysis of different chemical schemes in terms of complexity for n-heptane, which is the surrogate mono-component chosen as substitute for diesel due to its level of cetane. The main objective is to determine the effect of the kinetics mechanism in the simulated dynamics of combustion. Two different mechanisms have been tested for this study. On the one hand, the one proposed by Liu et al. [50] which consists of 44 species and 112 reactions and was developed specifically for on high-pressure non-premixed autoignition conditions. On the other hand, a more detailed mechanism such as that of Seiser et al. [51] was implemented. The mentioned mechanism consists of 159 species and 770 reactions.

Figure 3 reflects the results of heat release rate (HRR) and integral heat release (iHR) for Liu and Seiser mechanisms compared to the experimental data. The analysis of the different chemical schemes has been carried out for a reference set of operating conditions explained in detail in the Section 2.2. Figure 3 shows that both mechanisms (Liu and Seiser) are close to the experimental data in terms of iHR, with Liu mechanism being slightly more precise. As far as HRR is concerned, both mechanisms differ from the experimental behaviour predicting an ignition about 1 ms later than the value measured experimentally. Seiser mechanism provides slightly earlier ignition. In order to elaborate on its ability to describe low temperature combustion the temporal evolution of formaldehyde (CH_2O) was investigated. Figure 4 displays that both mechanisms predict exactly the same start of formalde-

hyde production. Therefore, the earlier ignition forecasted by the mechanism of Seiser et al. is not related to CH_2O production. Since the differences between the tested mechanisms proved to be minor, the skeletal mechanism of Liu et al. [50] was chosen to implement and perform the following analyses in order to reduce the computational cost.

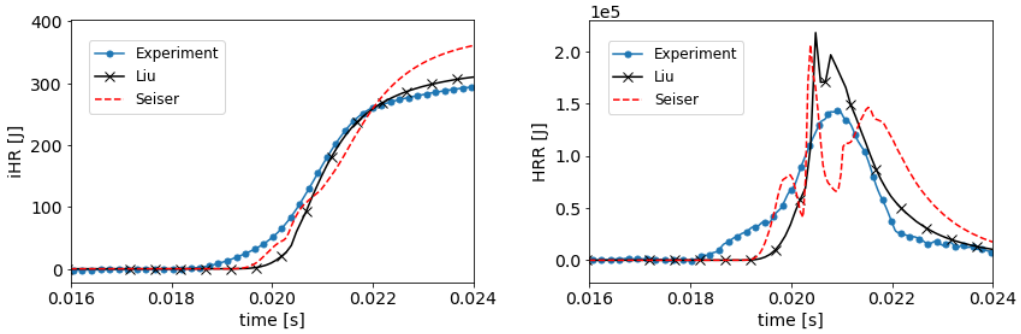

(a) Integral heat release (b) Heat release rate

Figure 3: Integral heat release and heat release rate as a function of time after the start of measurement for different chemistry mechanisms.

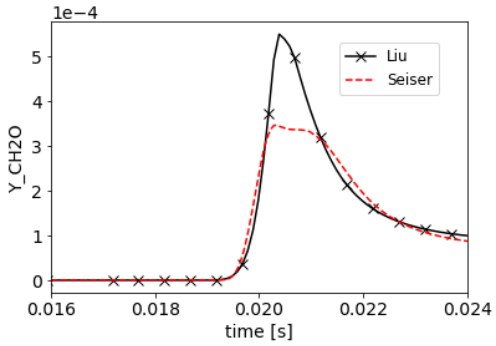

Figure 4: Formaldehyde mass fraction as a function of time after the start of measurement for different chemistry mechanisms.

3.1.4. Wall film modeling

There are a large number of researches focused on the study of the physics behind spray-wall collision, many of which can be extrapolated to real engine

applications. The spray-wall interaction mainly depends on the spray momentum and the energy exchange between the spray and the environment, therefore, the position of the injector in relation to the wall, its inclination and the operating conditions affect this phenomenon to a great extent [52]. In the present study and owing to the studied operating conditions (explained in detail in Section 2.2), the incoming spray experiences a low-density environment so the penetration is expected to be higher. As consequence, a large part of the fuel impinges the wall and creates a thin liquid film. The effect of incorporating detailed wall film modeling compared to the implementation of a faster full fuel rebound model proved to be significant both with respect to the mixing in the near wall region and to the long term integral heat released during combustion. For these reasons, it is concluded that incorporating film modeling is necessary for reliable results [53]. Therefore, the present study includes wall modeling using O'Rourke film splash model based on the Weber number, film thickness and viscosity.

3.2. Computational domain and mesh. Initial and boundary conditions

For this work, a detailed three-dimensional (3D) model of the RCEM available at ETH-Zürich was developed. This RCEM has been previously used in several experimental works [3, 35]. The main objective of this precise geometry is to accurately reproduce all the effects and behavior of the flow in order to compare and validate them with the experimental data available. Figure 5 illustrates each of the parts defined in the domain as well as the position of the injector used for the generation of the PCCI strategy conditions which, as mentioned above, is mounted on the perimeter of the cylinder and inclined 5º with respect to it.

The boundaries of the domain have all been defined as walls and designated as non-slip conditions and modeled using the Werner and Wengle wall function. The installation of temperature sensors in the experimental set-up allows differentiating between two temperatures on the walls. The upper part of the cylinder, which includes the area of the second injector, the threaded bores and the pressure switch adapter, is at a temperature of 388 K, while the rest of the walls have a slightly lower temperature of 378 K. The computational domain was defined as a single region filled with air (77% N_2 and 23% O_2). The mentioned region has been initialized, in terms of pressure and temperature, following the specified guidelines corresponding to each operating conditions defined for this study in the Section 2.2. Turbulence condition is specified by the turbulent kinetic energy with a value of

1 m^2/s^2.

The scope of the current work involves transient simulations in order to simulate the movement of the piston and the compression inside the cylinder caused by it. The lower part of the geometry, which corresponds to the moving piston, follows the physical movement displayed in Figure 2. It should be mention that this motion is identical for the OPs 1, 2 and 4. In order for this movement to be possible and the flow of fluid within regions to be controlled/prevented, a seal between the piston skirt and the liner has been defined. This method creates an unrealistic crevice volume between the piston and the cylinder liner.

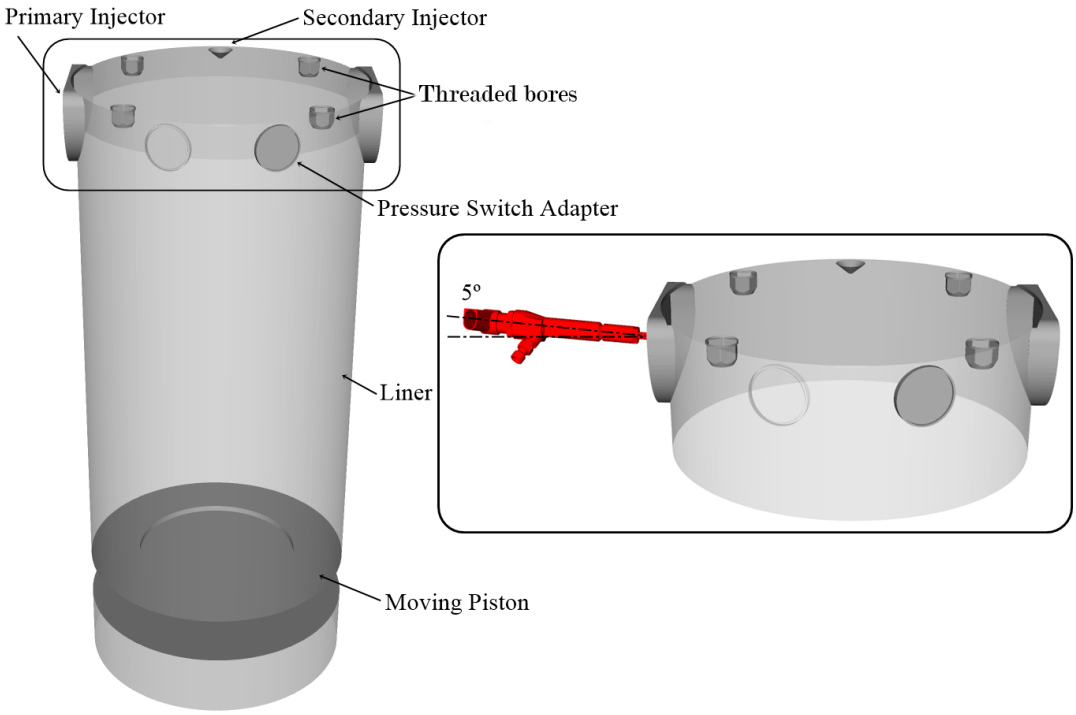

Figure 5: Sketch of the computational RCEM domain used for the CFD simulation.

CONVERGE is a novel program that reduces the time required for the mesh generation. It automatically generates a perfectly orthogonal, structured grid at run-time, based on simple, user-defined grid control parameters. Additionally, an Adaptive Mesh Refinement (AMR) algorithm could be utilized. The use of LES models implies a high dependency on cell size in energy

modeling. The width of the filter is directly related to the grid resolution and thus to the AMR algorithm. For that reason, it should be part of the overall LES methodology to define the reliance of predictions on the filter width. The final objective of this analysis is to obtain a resolved turbulent energy above a specified tolerance. This study was carried out and is presented in the Section 3.3. The choice of the final mesh size and refinements are based on compliance with the quality criteria explained in the mentioned section. Figure 6 displays the final configuration for OP1 through two different perspectives at 3.7 ms after 190 mm piston clearance. The selected base size is 2 mm. A fixed cone at the outlet of the injector has been defined in order to make the injection process easier and more precise. Moreover, the walls have been refined using two boundary layers of 0.5 mm to improve the prediction in the area. Finally, the AMR technique has been activated based on both variables: velocity with a criterion of 0.1 m/s as well as temperature with 2.5 K of sub-grid criteria. The minimum cell size takes place inside the cylinder and has a value of 125 µm. The resulting mesh has a maximum cell count around 30 million. The sprays are resolved with roughly 300000 parcels and the total computational cost lies between 32000 and 40000 CPU hours.

3.3. LES quality assessment

The turbulent determination in scale-resolved large eddy simulations (LES) is strongly influenced by the grid resolution and the modeling of the small scales. The interest of CFD researchers in the application of LES concepts to the investigation of in-cylinder flow phenomena has increased over the years. The implementation of these models requires quality assessment to provide adequate resolution of the turbulent flow energy and accurate results. The resolution of the grid is an important factor to take into account since it not only influences the contribution of the sub-grid scale model, but also the numerical discretization error. Numerous researchers have combined their efforts to define quality indexes that determine the numerical and model accuracy [54, 55]. For the ongoing research, the criteria selected to assess the consistency of the model would be one of the most widespread on the basis of the viscosity specified by the model of Celik et al. [56].

- *Index based on the viscosity*: this criterion is based on Equation 12 and evaluates the contribution relative to the laminar viscosity (υ), the sub-grid viscosity (υ_{sgs}) and the numerical viscosity (υ_{num}) to the quality assessment. Celik et al. [57] suggested that IQ_v values between 0.70

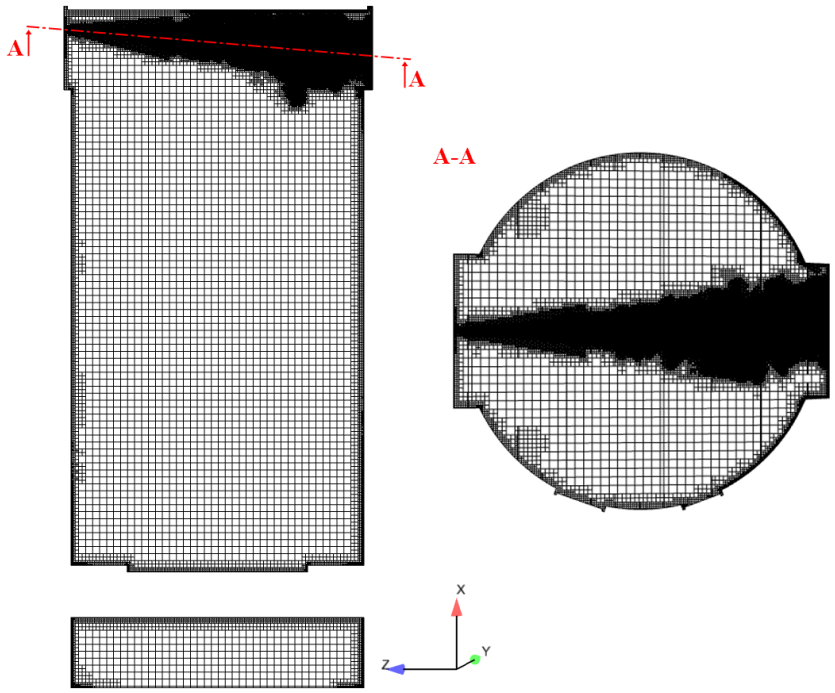

Figure 6: Mesh details in a vertical cross section and a plane along the injection direction.

and 0.80, which means at least 70% of the turbulent kinetic energy is resolved, can ensure appropriate LES quality for in-cylinder High-Reynolds-number flows.

$$IQ_{\upsilon} = \frac{1}{1 + \alpha_{\upsilon}(\frac{s^*}{(1-s^*)})^n} \tag{12}$$

Where s^*, always less than 1, can be defined by Equation 13.

$$s^* = \frac{\langle \upsilon_{sgs} \rangle + \langle \upsilon_{num} \rangle}{\langle \upsilon_{sgs} \rangle + \langle \upsilon_{num} \rangle + \langle \upsilon \rangle} \tag{13}$$

The two constants which appear in Equation 12 have been calibrated at $\alpha_{\upsilon} = 0.05$ and $n = 0.53$ based on DNS outcomes [58]. Typically, the evaluation of $s*$ requires the calculation of turbulent statistics.

In the present case, the problem does not have any stationary phase and due to the computational cost of a single realization, ensemble average is not practical for this sort of analysis. Therefore, this study has been carried out in each time-step for the transient simulation. Figure 7 displays one of the most sensitive moments in terms of quality corresponding to the first injection where the injected mass is higher than the split injections. The left side of the image shows the overall quality criterion while the right side of the image is saturated to indicate quality limits. The criterion proposed by Celik et al. is fulfilled along the plane of interest. It is also noticed that in the areas close to the walls the quality of the mesh is higher and this is related to the near-wall mesh refinement in the axial and both transversal directions of the spray applied to correctly capture the wall impingement. There is a small area near the injector where this criterion is not satisfied, corresponding to the area with the highest velocity in the domain. For such simulations, agreement has to be reached on the size of the refinement in order to meet the concentration criteria of the parcels. This, together with the fact that the interest of the study is the mixing and combustion zone, this quality has been assumed as suitable for the study.

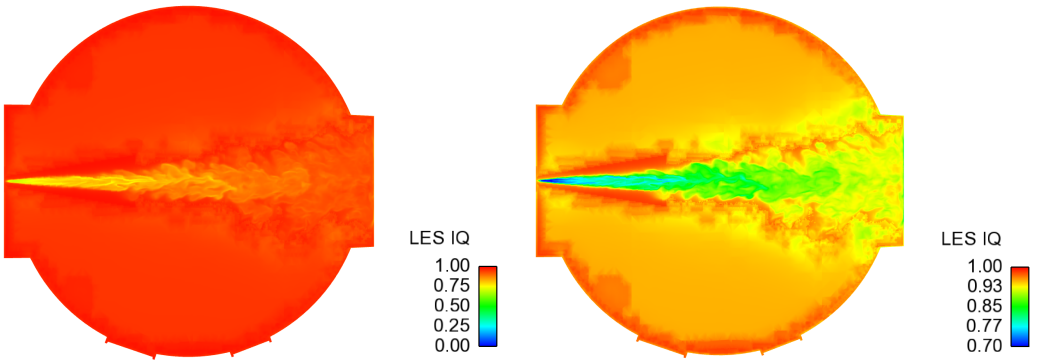

Figure 7: LES quality assessment based on the viscosity criteria at 3.7 ms after 190 mm piston clearance represented at plane A-A.

3.4. Validation experiments

The results of this research have been validated with experimental data obtained previously in the department [3]. Two different campaigns were carried out: reactive and non-reactive. The non-reactive campaign was based on the influence of multiple injections in the air-fuel mixture. On the other

hand, the reactive campaign focused on ignition and combustion behavior. For the non-reactive campaign, the Schlieren and Mie Scattering techniques were used in combination with a tracer substance at a concentration of 1.5 g/l (TMPD) PLIF [37]. The reactive campaign was developed with Schlieren, OH^* chemiluminescence as well as CH_2O PLIF imaging. For both reactive and non-reactive campaigns, the start of image acquisition was externally (position) triggered when the working piston reached a distance of 190 mm to the piston head. All measurements were performed out at 10 kHz repetition rate. Further details about measurement techniques, characteristics and configuration can be found in [3].

4. Results

4.1. Jet metrics validation

This section is mainly focused on the validation of the computational results in terms of jet penetration. The first injection is fast and the optical access limited, so there is no experimental data to validate it. Prior experimental studies [3, 26, 59] have shown how this first injection modifies the local flow characteristics, generating higher mixing and longer penetrations of the successive injections. The surrounding gas is accelerated in the direction of the spray, so the following injections benefit from the momentum and turbulence generated, penetrating further. This effect is known as slip-stream and may explain why the penetration length of the subsequent injection event is longer than previous one. However, it should be mentioned that although this occurs in constant volume chambers (CVC) studies [26, 59] and is observed here (Figure 8) [3], this behavior does not necessarily appear in real engine conditions. As long as the injection process occurs during the compression stroke, the operating conditions are different, with an environment of higher pressure and density, which together with the chemical reactions of the first and second impulse counteract the impulse gain and thus diminish the axial penetration of the spray. The successful prediction of the complicated spray evolution illustrates the validity of the hydrodynamics modeling employed in the numerical methodology and proves that mixing dynamics are accurately calculated in the simulations. It is observed that, despite correctly capturing the behaviour of the spray and affirming that the mixing dynamics are correct, there are certain differences between the computational and experimental results. The reasons for these discrepancies may be several, but among them the one that stands out is that the pulses

used and therefore the mass injected is so small that a slight variation in the acquisition process (data from the experiments) can completely change the spray. Not only that, but also the experimental techniques use a specific procedure for the calculation of the spray penetration and, while it is true that computational attempts are made to reproduce the calculation method, small discrepancies between techniques can lead to differences in the results. Experimental variability is notable in studies of this type and although the search for accuracy is interesting and possibly one of the main objectives of computational studies, it is not absolutely necessary to seek exact numerical values but it is also interesting to pay attention to trends, model capabilities and limitations.

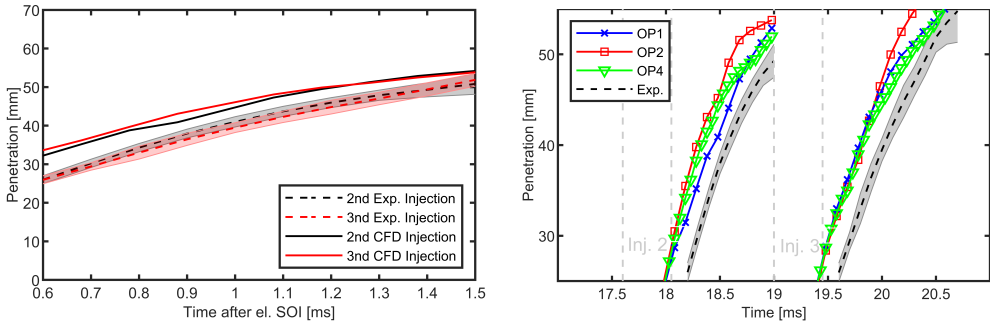

(a) OP1. (b) OP1, OP2 and OP4.

Figure 8: Jet penetration length for 2nd and 3rd in all operating conditions compared to experimental data.

Figure 8b depicts the temporal evolution of the penetration for both 2nd and 3rd injection in all the operating conditions studied and compares them with the respective average over all OPs. The average of all operating conditions has been chosen for comparison since, as demonstrated in [3], the experimental penetration results obtained did not differ between operating conditions for the 2nd and 3rd injection. It should be mentioned that the spray model constants were calibrated using OP1 and used unaltered for OP2 and OP4. Despite the difference in operating conditions, the evolution of the penetration length is almost similar for the studied cases. Whereas for OPs 1 and 4 the behavior is almost identical, especially in the last injection, OP2 seems to reflect a small difference. For this case (OP2), where the injected mass in the first injection is higher, a larger penetration is observed in the final instants represented. In addition, the aforementioned "slipstream"

effect is more pronounced for this operating condition.

4.2. Mixing dynamics

4.2.1. Local mixing phenomena

This section is mainly focused on analyzing the behavior of the local mixture dynamics in the 2nd and 3rd injection. While for the experimental analysis several repetitions were performed due to the limited precision of the single-shot, for the computational case and due to its high computational cost as mentioned above, the results presented are obtained from a single sample. Figure 9 illustrates the comparison between the equivalence ratio maps of the 2nd (upper half) and 3rd (lower half) injection for the reference OP1 condition. As the second and third injection pulses are identical for all OPs studied, similar dynamics were expected and also observed for OP2 and OP4, and are therefore not reproduced here. In the same way that was done experimentally [3], and in order to compare or make a similarity in the behavior between computational and experimental results, a threshold of $\Phi = 0.5$ has been applied, thus enhancing the contrast of the spray contour with the environment (white part in Figure 9).

The mixing fields presented in Figure 9 support the results reported in Section 4.1. The 3rd injection has a greater penetration because it benefits from the momentum and aerodynamic effects of the injection that precedes it. In fact and in spite of having applied the filter corresponding to the equivalence ratio to determine in a clearer way the spray contours, in the lower half part of the image (3rd injection) there are still some spots of equivalence ratio probably belonging to the previous injection. At a certain point in the injection process, 1.08 ms aSOI, the 3rd injection is observed to slow down as the benefits obtained from the previous injection are damped by the increase in density during the compression stroke. Another interesting effect observed in the cross-sectional average equivalence ratio profiles is the sharp drop at the injector tip in the 2nd injection while the 3rd injection shows a smoother decrease. The predicted drop in the equivalence ratio is associated with the formation of a stagnation plane which is characteristic of pulsed jets emerging in a quiescent environment [59]. On the other hand, the effect of the moderate drop in the equivalence ratio is once again due to increased mixing at the jet tip due to the effect of the previous injection [60].

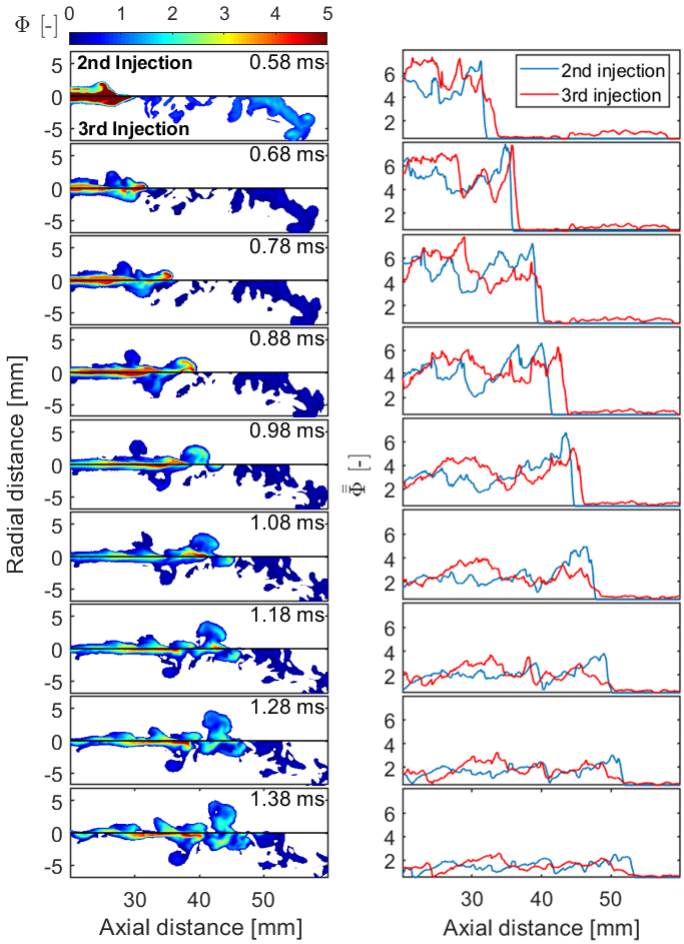

Figure 9: (Left) Comparison of the equivalence ratio Φ profiles of 2^{nd} and 3^{rd} injection for several time steps after the SOI (Start-of-Injection) of each injection respectively. (Right) Cross sectional average equivalence ratio $\bar{\bar{\Phi}}$ comparison between the 2^{nd} and 3^{rd} injection.

4.2.2. Global mixing state

For the present analysis, the global mixing state has been studied through the use of probability density functions (PDFs) of the equivalence ratio. The maps generated for the different operating conditions are displayed in Figure 10. Each column of the PDF maps represents the probability of the equivalence ratio to occur at a certain time step and it is indicated by the color map in logarithmic scale.

Maps are plotted as a function of time after 190 mm of piston clearance

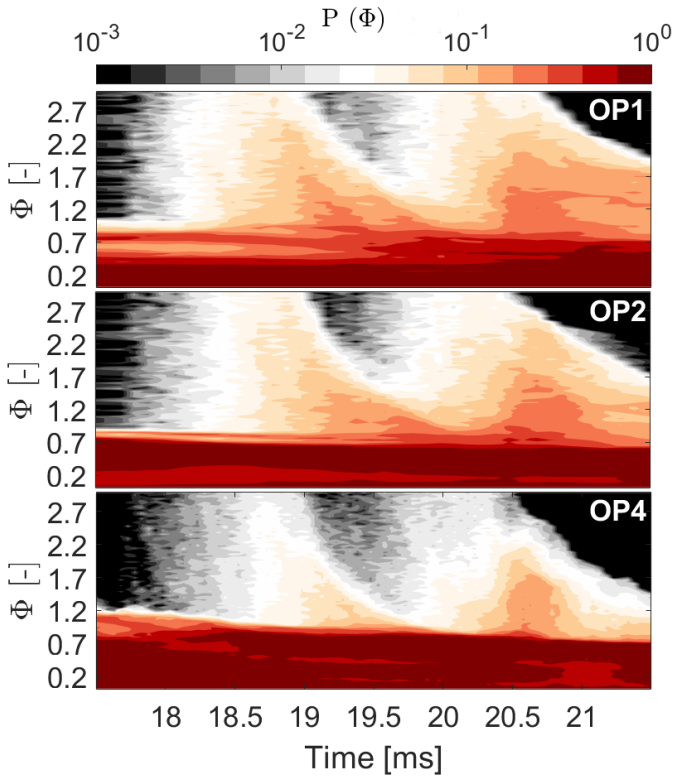

Figure 10: PDF maps of the equivalence ratio for all the operating conditions. The color map in logarithmic scale represents the probability that a given equivalence ratio (y-axis) occurs at a specific time step (x-axis) after the 190 mm of piston clearance.

so the results before 18.1 ms correspond to the base load of the first injection. Similar to the experimental results, the mixing at OP1 has a maximum probability around $\Phi = 0.5$ and minimum or no noticeable contributions beyond $\Phi = 1.2$. OP2 presents analogous distributions, but slightly moved to higher equivalence ratios, $\Phi = 0.7$, due to the doubled length of the base load injection. These two previous cases (OP1 and OP2) have a similar behavior to the experimental ones but in OP4 the computational results do not reflect such a pronounced stratification due to the delay of the first injection. This seems to demonstrate that fuel-air premixing is computationally faster than the experiments. After the time of 18.1 ms (0.5 ms aSOI of the 2^{nd} injection), there is a steep probability structure related to the 2^{nd} injection. This distribution reveals the wide range of equivalence ratio magnitudes of the above-

mentioned injection, which are rapidly reduced due to the momentum-driven mixing effect. It is noticed that in OP1 and OP2 the equivalence ratio has values lower than 2.5, whereas for the OP4 this value is well below, $\Phi \simeq 1.5$. After 19.5 ms corresponding to 0.5 ms aSOI of the 3rd injection, equivalence ratio structures and behavior similar to those mentioned above are observed.

Despite differences between operating conditions in the characteristics of the 1st injection, resulting in variations in the premixing state inside the studied volume, the state of the mixture after the third injection does not appear to differ between conditions. This suggests that it is the two post injections, identical for all research conditions, that determine the mixing in the plane of interest. Therefore, it is expected that the differences that might be observed in the section on ignition and combustion processes are related to local effects and not at the global mixing level.

4.3. Combustion analysis

4.3.1. Thermodynamic analysis and global combustion metrics

The thermodynamic analysis in the form of integral heat release (iHR) is depicted and compared to the experimental data in Figure 11. Although the phenomena of the ignition and the initial part of combustion are complex and difficult to be modeled, the evolution of combustion is captured successfully for the cases considered. For OP1 and OP4, the simulation predicts a delay in the ignition process of about 1 ms compared to the experimental measurement. Whereas in OP2, although there is a small lag in the CFD data, ignition occurs at similar time with both approaches. The trends of the iHR curves agree with the experimental ones in the case of OP1 and OP2. Whereas, simulation of OP4 shows computationally a steep slope of the heat release value. Capturing the exact ignition evolution accurately for all cases under study is an extremely difficult task considering the interplay of turbulence, spray dynamics, evaporation and chemistry. On top of it, computational feasibility necessitates modeling with many assumptions and adjustable constants. The existence of the mismatches between computational and experimental results could not be easily attributed to a specific source of uncertainty in the modeling process. The limitations of the chemical mechanisms at the low temperature limit and their inaccuracy in predicting CH_2O production early enough during the low temperature combustion regime (both mechanisms were developed for general purpose use) render them a strong candidate for the source of discrepancy.

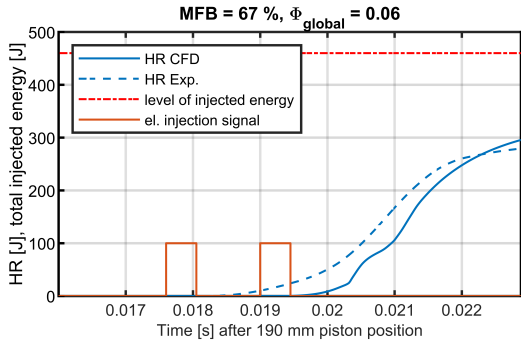

(a) OP1

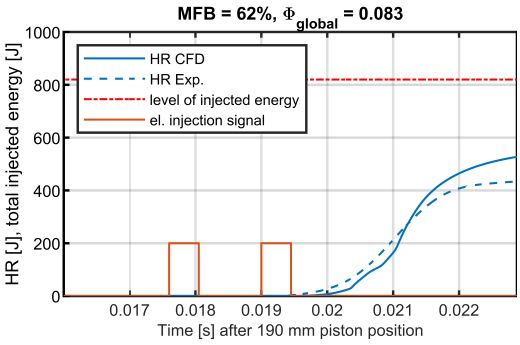

(b) OP2

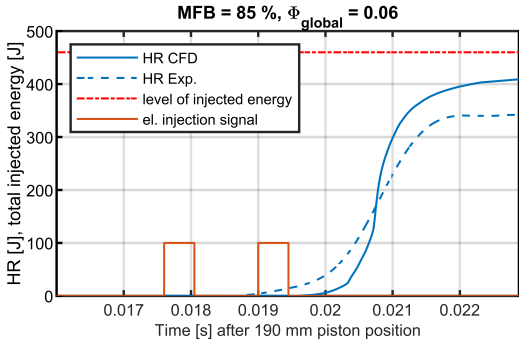

(c) OP4

Figure 11: Thermodynamic analysis using the integral Heat Release (iHR) for all the operating conditions.

The accumulated heat release is far below the level of injected energy in all the OPs, where injected energy is defined as the total mass injected multiplied by the calorific value of the fuel. In the case of OP1, the mass of fuel burnt (MFB) differs from the experimental result of 66%, in absolute value, by about 1%. On the contrary, OP2 and OP4 report a higher computational MFB value, showing an absolute difference of 7% in the case of OP2 (55% experimental MFB) and 10% in OP4 (75% experimental MFB). OP2 injects the double mass in the first injection compared to OP1, resulting in a richer mixture so that the absolute amount of fuel burnt is higher. The OP4 has a later first injection which results in a less homogeneous mixture when the second injection starts. This leads to the post injections (2^{nd} and 3^{rd}) encountering a richer mixture resulting in a larger MFB and a steeper iHR.

4.3.2. Ignition characteristics

The ignition process and the effect of multiple injections on mixing have been analyzed by a sequence of time-lapse images representing the mixture mass fraction of each injection separately and the mass fraction of CH_2O presented in Figure 12. In the experiment, the fuel distribution was measured by means of LIF, providing spatial information of the variable itself. In the simulation, in addition to evaporating to the fuel scalar, the corresponding source term due to evaporation has also been provided to three passive transported scalars, namely three mixture fractions, one for each injection event. This allows for discerning the fuel stemming from each one of the pulses in the overall distribution. The outcomes of this analysis are displayed in the plane of interest, parallel to the injection axis, at the same global time which has been displayed relative to each injection, aSOI of the 2^{nd} injection in green ($aSOI_2$) and aSOI of the 3^{rd} injection in black ($aSOI_3$), in the three operating conditions treated (OP1, OP2 and OP4). The mixture fraction corresponding to the 1^{st} injection is shown in yellow, the 2^{nd} injection in green and finally, the 3^{rd} injection in white. In addition, the mass fraction of formaldehyde is represented in red and is a good indicator of the ignition process. The first and most outstanding difference between the three OPs is the distribution of the mixture fraction corresponding to the 1^{st} injection. Considering the characteristics of each of the OPs, OP2 injects the first shot at the same time as OP1 but the injection time and thus the amount of mass injected is longer. On the other hand, OP4 has the same injected mass but this first shot occurs very close to the post injections. Both OP1 and OP2 have enough time to carry out a homogeneous mixing throughout the study volume, while OP4, on the other hand, has very close injections in time to each other, which makes it impossible for the mixing to be comparable to the other OPs.

Regarding OP1, the first early injection impinging the walls at high velocity thus distributing the fuel throughout the volume and generating a uniform concentration with similar values observed near the walls and in the centre of the cylinder. It is observed that the first spots of a noticeable CH_2O mass fraction can be seen in a diffuse form at time 2.08 ms $aSOI_2$ and brighter at 2.18 ms $aSOI_2$ while experimentally the first samples of formaldehyde are found at time 1.4 ms $aSOI_2$ [3]. Therefore, as seen in the Section 4.3.1, the ignition process in the computational case takes place at a later time than experimentally. At this time, the mixture and thermodynamic state seem

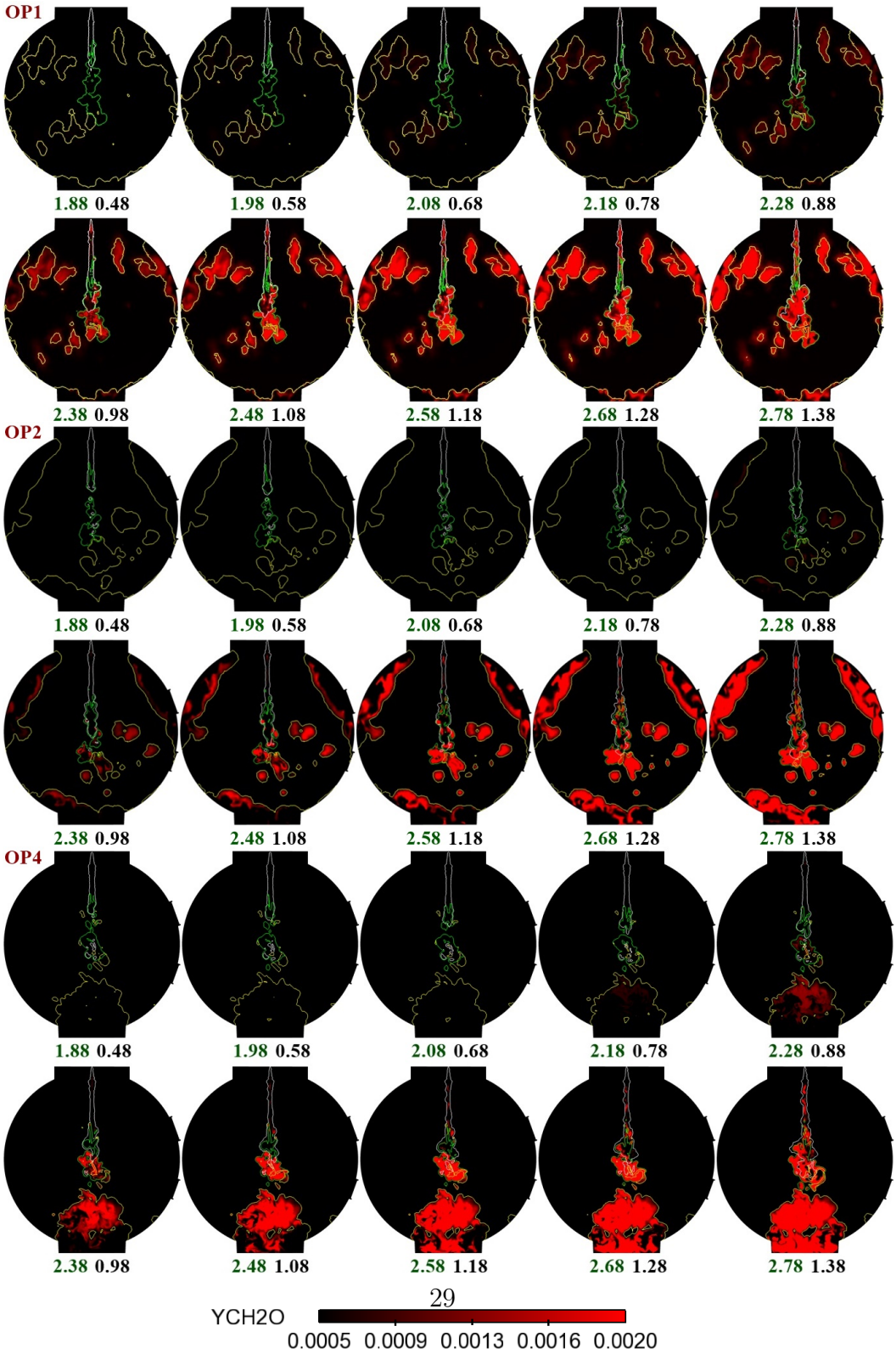

Figure 12: Time-resolved ignition dynamics. Superimposed mixture fraction of each injection, first injection (yellow), second injection (green) and third injection (white) together with mass fraction of CH_2O. Numbers below the image denote the time aSOI of the second injection in green and the third injection in back.

to be optimal to enhance the LT ignition which initially occurs in the mass fractions corresponding to the 1st injection and which are located in the cylinder surrounds. Microseconds later, at 2.28 ms $aSOI_2$, the concentration of formaldehyde becomes significant in pockets of fuel injected either during the second injection or in the areas of mixing of the 2^{nd} and the 3^{rd} injections. The temperature is still low in these areas so the high temperature combustion has not been achieved yet. Formaldehyde generation increases with time until at 2.78 ms $aSOI_2$ when the first high temperature combustion occurring spots appear. At the final stages of the process, the fuel concentrates in the near wall region because the first injection undergoes high temperature combustion as well. These high temperature spots appear mainly at the tip of the 3^{rd} injection and later, at the final stages of the process.

The behavior of OP2 is similar to that described above. In this operating condition, there is also a concentration of fuel near the walls belonging to the first injection. As in the experimental case, the appearance of the first formaldehyde spots occurs at a later time than in OP1, in this case 0.2 ms later. This effect may be due to a lower compression ratio in OP2 which causes a slower temperature rise inside the cylinder. On the other hand, the duration of the first injection leading to a higher mass injection results in richer mixtures so that the equivalence ratio is high and the temperature is too low to start LT oxidation. The first signs of CH_2O mass fraction come in areas corresponding to mixture fraction of the 1^{st} and 2^{nd} injections and later extend to areas belonging to the 3^{rd} injection. The temperature remains at low values until the first signs of high combustion temperatures emerge at 2.88 ms $aSOI_2$. In the time sequence presented, for this operating condition, the time of the start of combustion is not visible. Following the same behavior as OP1, the first hot spots appear near the tip of the 3^{rd} injection and quickly spread all over the spray and the areas near the walls.

Finally, with respect to OP4, what stands out in this sequence of images is the difference in the mixing pattern where the proximity between the 1^{st} and the two consecutive injections means that there is not enough time to promote a homogeneous mixture similar to those seen previously in OP1 and OP2. This closeness between injections may cause the 2^{nd} jet to entrain less fuel in the upstream regions of the spray, so that the equivalence ratio remains below the LT ignition limit. In fact, the first samples of CH_2O product of LT oxidation reactions appear mainly in the mixture fraction of the 1^{st} injection accumulated in areas close to the wall where the impingement of the mentioned injection takes place. This happens at 2.18 ms $aSOI_2$, but

quickly this formaldehyde formation spreads to areas at the tip of the 2nd injection first and to the whole jet later. The temperature at this time is low and it is not until 2.78 ms aSOI_2 that the first signs of high temperature combustion appear at the tip of the 3rd injection. Soon, as in the previous cases, the high temperatures spread to the other areas of the studied volume.

5. Conclusions

This research is mainly based on the study of the influence of multiple injection strategies on the mixing, ignition and combustion processes in a RCEM under PCCI relevant conditions. The effects of turbulence, which are important in this type of approach, have been characterized by LES approach. The split injection strategy consists of a main injection at the beginning of the compression stroke followed by two short injections near TDC, and it is used to generate the stratification and mixing conditions required by the novel PCCI combustion model. Despite minor differences in the overall equivalence ratio or compression ratio between the operating conditions studied, variations in local fuel-air mixing as well as ignition and combustion behavior were observed. The main findings of the analysis focus on the short double injection and are summarized below,

- The implementation of high fidelity simulations where turbulence is addressed from LES models allows accurate prediction of spray development and mixture formation during the injection process. The mentioned precision of the results has been ensured by meeting the viscosity-based quality criterion proposed by Celik in which the resolved energy of the system is greater than 70% of the total.

- Validation of the jet metric demonstrates that in consecutive injections the first one modifies the local flow characteristics which has an impact on the next injection. This second injection has a higher mixing rate promoted by the momentum and turbulence generated by the previous injection, resulting in longer penetration. It is also observed that this effect is mitigated as the conditions inside the cylinder change. The increase, albeit small, in density during the compression stroke, in addition to the chemical reactions of the first and second pulses, counteracts the momentum gain. However, in the local mixing state study it was observed that there is a moderate drop in the equivalence

ratio in the subsequent injection compared to a sharp drop in the first injection which ensures an increase in mixing at the jet tip due to the effect of the multiple injections.

- From the global mixing state analysis, it was determined that the mixture at the end of the post-injections was similar in all the operating conditions studied despite the difference in the characteristics of the main injection. Thus, it seems that the overall mixing state is dominated to a greater extent by the post-injections, which are identical in all the operating strategies studied.

- The ignition analysis reveals how the OP1 and OP2, due to their early main injection in the compression stroke, allow a more homogeneous mixture to be generated in the cylinder before the post injections take place than the OP4. The time between the main injection and the post-injections in the latter operating condition (OP4) is shorter, thus allowing reduced time for the mixing process and generating a less homogeneous overall state than the other two tested conditions (OP1 and OP2). The presence of formaldehyde, related to combustion at LT, takes place at similar times in OP1 and OP4 while in OP2 a delay of about 0.2 ms is observed due to the difference in compression ratio of this operating strategy. High temperature combustion tends to begin initially at the tip of the 3rd injection in all OPs and quickly spreads throughout the spray and to areas close to the walls.

In summary, the conducted research demonstrates how small changes in the operating strategy have a significant influence on the local state of the mixture and thus on the overall efficiency and performance of the engine. It is therefore proposed as future studies to analyze these same strategies using a real engine geometry in which air movements such as swirl and tumble, air motions that can influence the mixture and global efficiency, are considered.

Acknowledgments

Authors would like to thank the FVV (Forschungsvereinigung Verbrennungskraftmaschinen — Research Association for Combustion Engines, project "Partially premixed diesel combustion with multiple injections", no. 1352) and from the Swiss Federal Office of Energy (grant no. Sl/501744-01). Additionally, the Ph.D. student María Martínez has been funded by a grant from

the Government of Generalitat Valenciana with reference ACIF/2018/118 with financial support from The European Union and a grant for predoctoral stays out of the Comunitat Valenciana with reference BEFPI/2020/057.

Abbreviations

AMR	Adaptive Mesh Refinement
BDC	Bottom Dead Center
CFD	Computational Fluid Dynamics
CFL	Courant-Friendrichs-Lewy
CI	Compression Ignition
CVC	Constant Volume Cell
DDM	Droplet Discrete Model
EGR	Exhaust Gas Recirculation
HCCI	Homogeneous Charge Compression Ignition
HRR	Heat Release Rate
ICE	Internal Combustion Engine
iHR	Integral Heat Release
KH	Kelvin-Helmholtz
LES	Large Eddy Simulation
LTC	Low Temperature Combustion
NTC	No Time Counter
OP	Operating Point
PCCI	Premixed Charge Compression Ignition
PDF	Probability Density Function
PISO	Pressure Implicit with Splitting of Operators
PLIF	Planar Laser Induced Fluorescence
RCEM	Rapid Compression Expansion Machine
RT	Rayleigh-Taylor
SI	Spark Ignition
SOR	Succesive Over-Relaxation algorithm
TDC	Top Dead Center
UHC	Unburned Hydrocarbons

References

[1] V. Bermúdez, J. M. Lujan, P. Piqueras, D. Campos, Pollutants emission and particle behavior in a pre-turbo aftertreatment light-duty diesel engine, Energy 66 (0) (2014) 509–522. doi:10.1016/j.energy.2014.02.004.

[2] B. K. Bose, F. F. Wang, Energy, Environment, Power Electronics, Renewable Energy Systems, and Smart Grid, Power Electronics in Renewable Energy Systems and Smart Grid (2019) 1–83doi:10.1002/9781119515661.ch1.

[3] U. Doll, C. Barro, M. Todino, K. Boulouchos, Impact of a split injection strategy on mixing, ignition and combustion behavior in Premixed Charge Compression Ignition combustion, Fuel (2021) 1–26.

[4] M. Krishnamoorthi, R. Malayalamurthi, Z. He, S. Kandasamy, A review on low temperature combustion engines: Performance, combustion and emission characteristics, Renewable and Sustainable Energy Reviews 116 (October) (2019) 109404. doi:10.1016/j.rser.2019.109404.

[5] D. Mei, L. Tu, S. Yue, D. Adu-Mensah, S. Jiang, Simulation of Combustion Process and Pollutant Generation in a PCCI Diesel Engine with Adaptable Multiple Injection, Journal of Energy Engineering 144 (5) (2018) 04018051. doi:10.1061/(asce)ey.1943-7897.0000568.

[6] K. Epping, S. Aceves, R. Bechtold, J. Dec, The potential of HCCI combustion for high efficiency and low emissions, SAE Technical Papers (724) (2002). doi:10.4271/2002-01-1923.

[7] M. M. Hasan, M. M. Rahman, K. Kadirgama, A review on homogeneous charge compression ignition engine performance using biodiesel-diesel blend as a fuel, International Journal of Automotive and Mechanical Engineering 11 (1) (2015) 2199–2211. doi:10.15282/ijame.11.2015.3.0184.

[8] S. C. Kong, R. D. Reitz, Use of detailed chemical kinetics to study HCCI engine combustion with consideration of turbulent mixing effects, Journal of Engineering for Gas Turbines and Power 124 (3) (2002) 702–707. doi:10.1115/1.1413766.

[9] H. Bendu, S. Murugan, Homogeneous charge compression ignition (HCCI) combustion: Mixture preparation and control strategies in diesel engines, Renewable and Sustainable Energy Reviews 38 (2014) 732–746. doi:10.1016/j.rser.2014.07.019.

[10] S. Gowthaman, A. P. Sathiyagnanam, The effect of exhaust gas recirculation on performance and emission characteristics of HCCI engine, International Journal of Ambient Energy 38 (2) (2017) 178–185. doi:10.1080/01430750.2015.1074616.

[11] R. J. Iverson, R. E. Herold, R. Augusta, D. E. Foster, J. B. Ghandhi, J. A. Eng, P. M. Najt, The effects of intake charge preheating in a gasoline-fueled HCCI engine, SAE Technical Papers 114 (2005) (2005) 1566–1574. doi:10.4271/2005-01-3742.

[12] T. W. Ryan, T. J. Callahan, D. Mehta, HCCI in a variable compression ratio engine-effects of engine variables, SAE Technical Papers (724) (2004). doi:10.4271/2004-01-1971.

[13] J. Hyvönen, G. Haraldsson, B. Johansson, Supercharging HCCI to extend the operating range in a multi-cylinder VCR-HCCI engine, SAE Technical Papers 112 (2003) 2456–2468. doi:10.4271/2003-01-3214.

[14] C. Wouters, T. Ottenwälder, B. Lehrheuer, S. Pischinger, M. Wick, J. Andert, D. Gordon, Evaluation of the Potential of Direct Water Injection in HCCI Combustion, SAE Technical Papers (December) (2019) 1–12. doi:10.4271/2019-01-2165.

[15] J. Valero-Marco, B. Lehrheuer, J. J. López, S. Pischinger, Potential of water direct injection in a CAI/HCCI gasoline engine to extend the operating range towards higher loads, Fuel 231 (November 2017) (2018) 317–327. doi:10.1016/j.fuel.2018.05.093.

[16] M. Murugesa Pandian, K. Anand, Comparison of different low temperature combustion strategies in a light duty air cooled diesel engine, Applied Thermal Engineering 142 (April) (2018) 380–390. doi:10.1016/j.applthermaleng.2018.07.047.

[17] Z. Peng, B. Liu, W. Wang, L. Lu, CFD investigation into diesel PCCI combustion with optimized fuel injection, Energies 4 (3) (2011) 517–531. doi:10.3390/en4030517.

[18] X. Liang, Z. Zheng, H. Zhang, Y. Wang, H. Yu, A review of early injection strategy in premixed combustion engines, Applied Sciences (Switzerland) 9 (18) (2019) 1–34. doi:10.3390/app9183737.

[19] J. M. Desantes, J. J. López, J. M. García-Oliver, D. López-Pintor, A phenomenological explanation of the autoignition propagation under HCCI conditions, Fuel 206 (2017) 43–57. doi:10.1016/j.fuel.2017.05.075.

[20] J. M. Desantes, J. J. López, S. Molina, D. López-Pintor, Theoretical development of a new procedure to predict ignition delays under transient thermodynamic conditions and validation using a Rapid Compression-Expansion Machine, Energy Conversion and Management 108 (2016) 132–143. doi:10.1016/j.enconman.2015.10.077.

[21] S. L. Kokjohn, R. M. Hanson, D. A. Splitter, R. D. Reitz, Experiments and modeling of dual-fuel HCCI and PCCI combustion using in-cylinder fuel blending, SAE International Journal of Engines 2 (2) (2010) 24–39. doi:10.4271/2009-01-2647.

[22] D. A. Pierpont, D. T. Montgomery, R. D. Reitz, Reducing particulate and nox using multiple injections and egr in a D.I. diesel, SAE Technical Papers (412) (1995). doi:10.4271/950217.

[23] M. Yao, H. Wang, Z. Zheng, Y. Yue, Experimental study of multiple injections and coupling effects of multi-injection and EGR in a HD diesel engine, SAE Technical Papers 4970 (2009). doi:10.4271/2009-01-2807.

[24] Y. Liu, R. D. Reitz, Optimizing HSDI diesel combustion and emissions using multiple injection strategies, SAE Technical Papers 2005 (724) (2005). doi:10.4271/2005-01-0212.

[25] J. V. Jose, M. Mittal, A. Ramesh, Effect of multiple injections on spray wall impingement in a small gasoline direct- injection engine -A CFD Analysis Effect of multiple injections on spray wall impingement in a small gasoline direct- injection engine – A CFD Analysis, 12th Asia-Pacific Conference on Combustion July 01, 2 (November) (2019).

[26] R. Payri, F. J. Salvador, R. Abboud, A. Viera, Study of evaporative diesel spray interaction in multiple injections using optical diagnostics, Applied Thermal Engineering 176 (May) (2020) 115402. doi:10.1016/j.applthermaleng.2020.115402.

[27] K. Mathivanan, J. M. Mallikarjuna, A. Ramesh, Influence of multiple fuel injection strategies on performance and combustion characteristics of a diesel fuelled HCCI engine - An experimental investigation, Experimental Thermal and Fluid Science 77 (2016) 337–346. doi:10.1016/j.expthermflusci.2016.05.010.

[28] Y. Lu, W. Yu, W. Su, Using multiple injection strategies in diesel PCCI combustion: Potential to extend engine load, improve trade-off of emissions and efficiency, SAE 2011 World Congress and Exhibition (2011). doi:10.4271/2011-01-1396.

[29] J. M. Desantes, J. M. García-Oliver, W. Vera-Tudela, D. López-Pintor, B. Schneider, K. Boulouchos, Study of the auto-ignition phenomenon of

PRFs under HCCI conditions in a RCEM by means of spectroscopy, Applied Energy 179 (2016) 389–400. doi:10.1016/j.apenergy.2016.06.134.

[30] D. Mitakos, C. Blomberg, A. Vandersickel, Y. Wright, B. Schneider, K. Boulouchos, Ignition Delays of Different Homogeneous Fuel-air Mixtures in a Rapid Compression Expansion Machine and Comparison with a 3-Stage-ignition Model Parameterized on Shock Tube Data, SAE International Journal of Engines 6 (4) (2013). doi:10.4271/2013-01-2625.

[31] J. M. Desantes, J. J. López, S. Molina, D. López-Pintor, Theoretical development of a new procedure to predict ignition delays under transient thermodynamic conditions and validation using a Rapid Compression-Expansion Machine, Energy Conversion and Management 108 (2016) 132–143. doi:10.1016/j.enconman.2015.10.077.

[32] A. Srna, B. von Rotz, K. Herrmann, K. Boulouchos, G. Bruneaux, Experimental investigation of pilot-fuel combustion in dual-fuel engines, Part 1: Thermodynamic analysis of combustion phenomena, Fuel 255 (November 2018) (2019). doi:10.1016/j.fuel.2019.115642.

[33] M. Bolla, E. Shapiro, N. Tiney, P. Kyrtatos, M. Kotzagianni, K. Boulouchos, Numerical simulations of pre-chamber combustion in an optically accessible rcem, SAE Technical Papers 2019-April (April) (2019) 1–11. doi:10.4271/2019-01-0224.

[34] D. López-Pintor, Theoretical and experimental study on the autoignition phenomena of homogeneous reactive mixtures, Ph.D. thesis, Universitat Politècnica de València (2017). doi:10.4995/Thesis/10251/90642.

[35] T. Kammermann, J. Koch, Y. M. Wright, P. Soltic, K. Boulouchos, Generation of Turbulence in a RCEM towards Engine Relevant Conditions for Premixed Combustion Based on CFD and PIV Investigations, SAE Technical Papers 2017-Septe (2017). doi:10.4271/2017-24-0043.

[36] S. Schlatter, B. Schneider, Y. Wright, K. Boulouchos, Experimental study of ignition and combustion characteristics of a diesel pilot spray in a lean premixed methane/air charge using a rapid compression expansion machine, SAE Technical Papers (2012). doi:10.4271/2012-01-0825.

[37] A. Srna, M. Bolla, Y. M. Wright, K. Herrmann, R. Bombach, S. S. Pandurangi, K. Boulouchos, G. Bruneaux, Effect of methane on pilot-fuel auto-ignition in dual-fuel engines, Proceedings of the Combustion Institute 37 (4) (2019) 4741–4749. doi:10.1016/j.proci.2018.06.177.

[38] Y. Park, C. Bae, Effects of single and double post injections on diesel PCCI combustion, SAE Technical Papers 1 (2013). doi:10.4271/2013-01-0010.

[39] P. G. Szymkowicz, J. Benajes, Development of a Diesel Surrogate Fuel Library, Fuel 222 (January) (2018) 21–34. doi:10.1016/j.fuel.2018.01.112.

[40] K. J. Richards, P. K. Senecal, E. Pomraning, CONVERGE v2.4, Convergent Science, Madison, Wi (2018).

[41] C. M. Rhie, W. L. Chow, Numerical study of the turbulent flow past an airfoil with trailing edge separation, AIAA Journal 21 (11) (1983) 1525–1532. doi:10.2514/3.8284.

[42] A. H. Kakaee, P. Jafari, A. Paykani, Numerical study of natural gas/diesel reactivity controlled compression ignition combustion with large eddy simulation and reynolds-averaged Navier-Stokes model, Fluids 3 (2) (2018). doi:10.3390/fluids3020024.

[43] S. Pope, Turbulent Flows, sixth Edition, Cambridge University Press, 2009.

[44] A. Yoshizawa, K. Horiuti, A Statistically-Derived Subgrid-Scale Kinetic Energy Model for the Large-Eddy Simulation of Turbulent Flows, Journal of the Physical Society of Japan 54 (8) (1985) 2834–2839. doi:10.1143/JPSJ.54.2834.

[45] S. Menon, P. K. Yeung, W. W. Kim, Effect of subgrid models on the computed interscale energy transfer in isotropic turbulence, Computers and Fluids 25 (2) (1996) 165–180. doi:10.1016/0045-7930(95)00036-4.

[46] P. K. Senecal, K. J. Richards, E. Pomraning, T. Yang, M. Z. Dai, R. M. McDavid, M. A. Patterson, S. Hou, T. Shethaji, A new parallel cut-cell cartesian CFD code for rapid grid generation applied to in-cylinder diesel

engine simulations, SAE Technical Papers 2007 (724) (2007) 776–790. doi:10.4271/2007-01-0159.

[47] D. P. Schmidt, C. J. Rutland, A New Droplet Collision Algorithm, Journal of Computational Physics 164 (1) (2000) 62–80. doi:10.1006/jcph.2000.6568.

[48] S. L. Post, J. Abraham, Modeling the outcome of drop – drop collisions in Diesel sprays, International Journal of Multiphase Flow 28 (2002) 997–1019. doi:10.1016/S0301-9322(02)00007-1.

[49] P. K. Senecal, E. Pomraning, K. J. Richards, T. E. Briggs, C. Y. Choi, R. M. McDavid, M. A. Patterson, Multi-dimensional modeling of direct-injection diesel spray liquid length and flame lift-off length using cfd and parallel detailed chemistry, SAE Technical Papers (724) (2003). doi:10.4271/2003-01-1043.

[50] S. Liu, J. C. Hewson, J. H. Chen, H. Pitsch, Effects of strain rate on high-pressure nonpremixed n-heptane autoignition in counterflow, Combustion and Flame 137 (3) (2004) 320–339. doi:10.1016/j.combustflame.2004.01.011.

[51] R. Seiser, H. Pitsch, K. Seshadri, W. J. Pitz, H. J. Curran, Extinction and autoignition of n-heptane in counterflow configuration, Proceedings of the Combustion Institute 28 (2000) 2029–2037. doi:10.1016/S0082-0784(00)80610-4.

[52] A. Montanaro, S. Malaguti, S. Alfuso, Wall impingement process of a multi-hole GDI spray: Experimental and numerical investigation, SAE Technical Papers (April) (2012). doi:10.4271/2012-01-1266.

[53] C. Michel, G. Rodrigues, Modelling of Spray-Wall Impingement (2016).

[54] J. Meyers, B. J. Geurts, M. Baelmans, Database analysis of errors in large-eddy simulation, Physics of Fluids 15 (9) (2003) 2740–2755. doi:10.1063/1.1597683.

[55] B. J. Geurts, J. Fröhlich, A framework for predicting accuracy limitations in large-eddy simulation, Physics of Fluids 14 (6) (2002). doi:10.1063/1.1480830.

[56] I. B. Celik, Z. N. Cehreli, I. Yavuz, Index of resolution quality for large eddy simulations, Journal of Fluids Engineering, Transactions of the ASME 127 (5) (2005) 949–958. doi:10.1115/1.1990201.

[57] I. Celik, I. Yavuz, A. Smirnov, Large eddy simulations of in-cylinder turbulence for internal combustion engines: A review, International Journal of Engine Research 2 (2) (2001) 119–148. doi:10.1243/1468087011545389.

[58] I. Celik, M. Klein, J. Janicka, Assessment measures for engineering LES applications, Journal of Fluids Engineering, Transactions of the ASME 131 (3) (2009) 0311021–03110210. doi:10.1115/1.3059703.

[59] S. Skeen, J. Manin, L. M. Pickett, Visualization of Ignition Processes in High-Pressure Sprays with Multiple Injections of n-Dodecane, SAE International Journal of Engines 8 (2) (2015) 696–715. doi:10.4271/2015-01-0799.

[60] G. Bruneaux, D. Maligne, Study of the Mixing and Combustion Processes of Consecutive Short Double Diesel Injections, SAE Technical Paper 2009-01-1352 (2009). doi:10.4271/2009-01-1352.

Appendix A. Adaptive Mesh Refinement (AMR) study

The proper grid resolution study as it is known in the literature refers to is the standard procedure in RANS. However, in LES, significant differences are expected every time the grid is refined since the scales of the resolved turbulent structures are dependent on the turbulence resolution length scale or filter width $\Delta_e(x)$ which is directly related to the grid resolution dx_k (the mesh is the filter in the current approach). That is why, other approaches were developed and are currently employed in the present research, such as the criteria established by Celik et al. Despite this, and in order to see the influence of the mesh on the results, a mesh sensitivity study was carried out using three different cases:

- *Case 1*: Base size: 2 mm; Embedding: 3 levels; Minimum size: 0.250 mm.
- *Case 2*: Base size: 2 mm; Embedding: 4 levels; Minimum size: 0.125 mm.
- *Case 3*: Base size: 1 mm; Embedding: 3 levels; Minimum size: 0.125 mm.

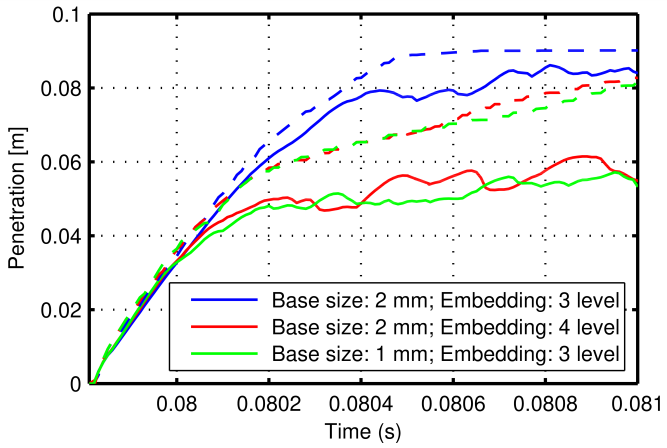

Figure Appendix A.1: Analysis of the influence of the Adaptive Mesh Refinement (AMR) for the reference operating condition OP1.

Comparing the macroscopic variable of penetration, there are visible differences between the three cases analyzed. The one with the lowest refinement (2 mm of base size and 3 levels of refinement) has a higher injection velocity, penetrating faster and evaporating less fuel. This causes, as shown in Figure Appendix A.1, a much earlier impact with the wall. Furthermore, if one looks at the mixture fraction contours and the particle velocity, the above statement is again corroborated. It can also be noticed in Figure Appendix A.2 that the spray aperture in *case 1* is much smaller and reflects less turbulent structures than *cases 2* and *3*. If computational cost is compared, the high resolution setup has minimum cell size of 125 μm and maximum cell count around 30 million. The sprays are resolved with roughly 300.000 parcels and the total computational cost lies between 32.000 and 40.000 CPUhours. The low-resolution setup has a minimum cell size of 250 μm and maximum cell count around 9 million. The computational cost for this case is below 10.000 CPUhours. The complex local interactions between physical and chemical processes dictates the use of high resolution for the production runs. These expensive calculations offer deep insights into the detailed evolution of phenomena that cannot be measured with experimental techniques and hence the information extracted is valuable.

Regarding the cases with the same minimum cell size (*case 2* and *case 3*), it can be observed that penetration has similar trends in both cases with cumulative errors of less than 4% and the spray shape as well as the particle velocity show similar results. In this particular scenario, offering similar results and with the aim of saving computational cost as these studies require a high computational capacity, the choice to carry out the study has been *case 2* (2 mm of base size and 4 levels of refinement).

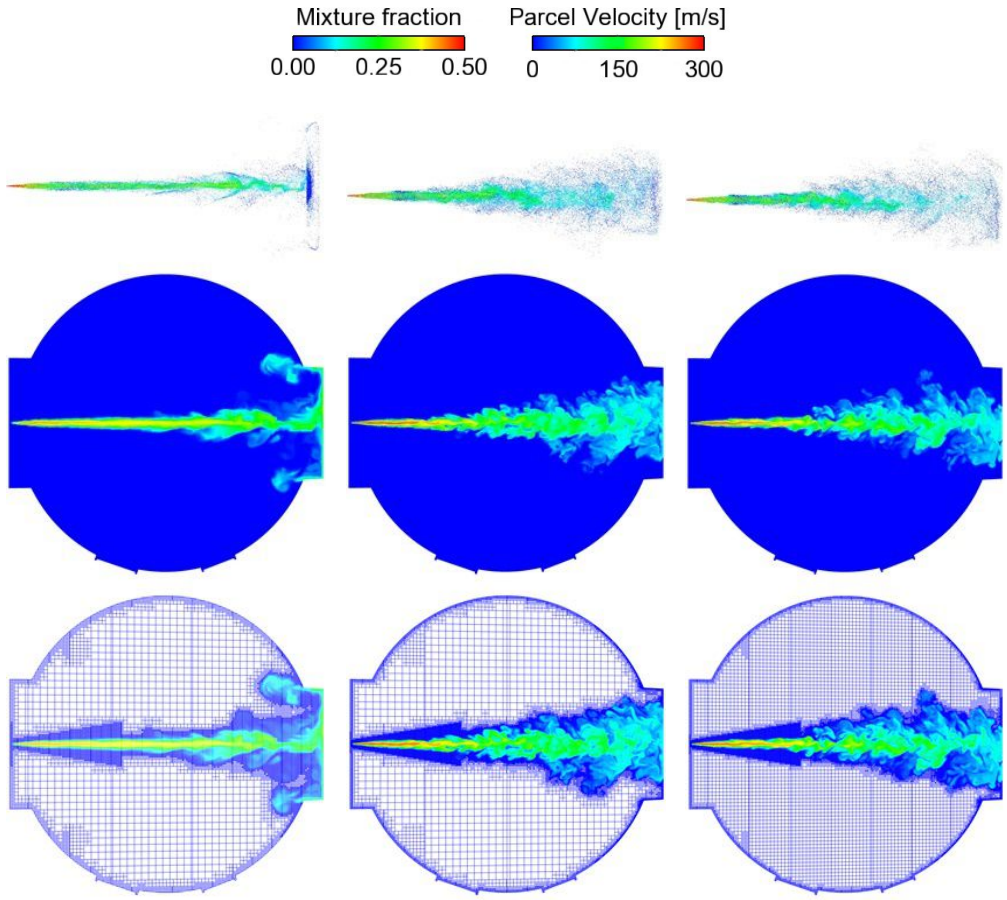

(a) 2 mm; 3 emb (b) 2 mm; 4 emb (c) 1 mm; 3 emb

Figure Appendix A.2: Mixture fraction and particle velocity for the three different analyzed cases at t = 0.0815 ms for the reference operating condition OP1.